<Research Report>Single crystal growth and magnetism of the kagomé-lattice Co-shandite

AUTHOR(S):

Kassem, Mohamed A.

CITATION:

Kassem, Mohamed A.. <Research Report>Single crystal growth and magnetism of the kagomé-lattice Co-shandite. 京都大学物性科学センター誌 : LTMセンター誌 2017, 31: 9-18

ISSUE DATE:

2017-12

URL:

https://doi.org/10.14989/228932

Single crystal growth and magnetism of the kagomé-lattice Co-shandite

Mohamed A. Kassem*
Department of Materials Science and Engineering, Kyoto University, Kyoto 606-8501, Japan.

Co-based shandites $Co_3M_2S_2$ (M = Sn and/or In) are candidates of quasi-two-dimensional (Q2D) magnetism showing exotic properties. The interest is implied by its layered crystal structure that contains 2D-kagomé networks of magnetic Co atoms with antisymmetric Dzyaloshinskii-Moriya (DM) interaction and possibly spin frustration. The magnetism of Co-shandites have been previously investigated mainly using polycrystalline samples to show interesting magnetic properties. However, no experimental study from the above-mentioned viewpoint, Q2D kagomé system, has been carried out. For this purpose, investigations using single crystals are essential. In our study of Co-shandites, we successfully grew single crystals of two series-compounds of Co-based shandites, $Co_3Sn_{2-x}In_xS_2$ and $Co_{3-y}Fe_ySn_2S_2$, to investigate them as the Q2D kagomé system and we found novel properties using the grown single crystals, such as the highly Q2D itinerant electron magnetism and low-field anomalous phase very close to T_C.

1. Introduction

Due to its layered crystal structure that contains 2D-kagomé networks of magnetic Co atoms, Co-based shandites show novel properties [1-4]. The layered crystal structure implies low dimensional character of its magnetism, as the long-range orders are destabilized at low dimensions, and hence, thermal and quantum fluctuations are strongly enhanced [5-11]. In viewpoint of magnetism, the 2D corner-sharing triangular lattice, i.e. kagomé lattice, of an antiferromagnetically coupled spin system is a representative frustrated lattice. For instance, the geometric spin frustration can exhibit a quantum disordered spin-liquid state [12] and novel magnetically ordered states with nontrivial spin textures [13-16]. Another interesting characteristic of the kagomé magnets is the asymmetric Dzaloshinski–Moriya (DM) interaction, which is acting also as a driving force to nontrivial spin textures [17-20] . For example, both ferro- and antiferromagnetic orders can be destabilized by the DM interaction resulting in spiral or canted spin structures. When the exchange interaction is principally ferromagnetic, further nano-scale objects of topologically-protected vortex-like spin texture, so-called 'skyrmions', may be realized by the DM interaction [21]. The search for new layered compounds of 2D-kagomé networks of magnetic atoms is a key to observe exotic phenomena.

The crystal structure of shandite compounds of the general formula $T_3M_2X_2$ (T = Ni, Co, Rh or Pd; M = In, Sn, Pb or Tl; and X = S or Se) which belongs to the trigonal space group $R\bar{3}m$ is shown in Fig. 1(a), illustrated by the VESTA software [22]. The T and X atoms occupy the unique Wyckoff positions 9*e* (1/2,0,0) and 6*c* (0,0,z), respectively, while the M atoms are distributed between two positions, $M1$: 3*b* (0,0,1/2) and $M2$: 3*a* (0,0,0). The shandite-type crystal structure consists of metallic layers stacked in ABC fashion along *c*-

* Present address : Department of Physics, Assiut University, Assiut 71515, Egypt

direction in a hexagonal notation. The layers are arranged in the kagomé sub-lattice of the *T* atoms and *M*2-triangular sub-lattice, shown in the bottom of Fig. 1(a). The layers are connected through *M*1 atoms that locate in polyhedra of trigonal antiprisms generated by the *T* atoms triangles.

Among shandite, $Co_3Sn_2S_2$ lonely shows a magnetic (ferromagnetic) order with a Curie temperature, $T_C \sim$ 172 K [23,24]. Strong uniaxial anisotropy of magnetization have been recently observed using single crystals grown out of Sn-flux [25] and by a modified Bridgman method [2]. The observed spontaneous magnetic moment, ~ 0.3 μ_B/Co along the easy axis at 2 K, is much smaller than the effective moment at higher temperatures than T_C, ~ 0.6 μ_B/Co, indicating weakly itinerant electron ferromagnetism. Co-based shandites, except for the parent compound $Co_3Sn_2S_2$ [2], have been investigated mainly using polycrystalline samples and some interesting properties have been reported such as, the half-metallic ferromagnetism [23,26,27], magnetic instability controlled by chemical substitution [24,26,28] and high thermoelectric properties [29-31]. Detailed investigations of Co-shandites as a Q2D kagomé system, strongly requires single crystals. In this article, we review our success in growing single crystals of two series-compounds of Co-based shandites, $Co_3Sn_{2-x}In_xS_2$ and $Co_{3-y}Fe_ySn_2S_2$, and results of subsequent investigations for its structure and magnetic properties as Q2D kagomé ferromagnets.

2. Experimental Details

Single crystals of two series-compounds of Co-based shandites, $Co_3Sn_{2-x}In_xS_2$ ($0 < x \leq 2$) and $Co_{3-y}Fe_ySn_2S_2$ ($y \leq 0.5$) used in the current study were grown out of Sn, In and/or Pb-fluxes as detailed in our previously published articles [32,33]. Furtherly, much larger single crystals of $Co_3Sn_{2-x}In_xS_2$ have been synthesized by a modified Bridgman method (not published). The grown crystals were characterized by powder XRD and their structure parameters were refined by the Rietveld method [34]. The chemical compositions and crystals axes were investigated by wave length dispersive X-ray spectroscopy (SEM-WDX) and Laue X-ray photohraphy, respectively. The magnetization and AC susceptibility measurements were performed using a SQUID magnetometer (MPMS, Quantum Design, installed in the LTM Center of Kyoto University) in a temperature range of 2–350 K with magnetic field up to 7 T. Two experimental regimes in the low-field magnetization and AC susceptibility, previously described Zero-field-cooled (ZFC) and field-cooled (FC) scans [4,35], have been followed. The spin relaxation processes at selected temperatures were systematically studied by measuring the ZFC AC susceptibility at different magnetic fields and in a frequency range of five orders of magnitude from 0.01 to 1000 Hz. Crystals with different shapes, sizes, and batches were used to check for the results reproducibility.

3. Results and Discussions

3.1 Crystal growth and structure of $Co_3Sn_{2-x}In_xS_2$ and $Co_{3-y}Fe_ySn_2S_2$

WDX has indicated a successful growth of stoichiometric single crystals of the whole range of *x* in $Co_3Sn_{2-x}In_xS_2$ and *y* up to ~ 0.5 in $Co_{3-y}Fe_ySn_2S_2$ (due to the limited solubility of Fe and absence of $Fe_3Sn_2S_2$ in nature [28]). Laue X-ray spectroscopy indicated high-quality grown crystals with the flat hexagonal plane is the *ab* plane [32,33]. Typically grown single crystals were imaged on a mm scale and are shown in the top inset of Fig. 1(b).

Figure 1(b) shows the room-temperature observed and calculated powder XRD patterns, as well as their differences, of representative *x* and *y* of $Co_3Sn_{2-x}In_xS_2$ and $Co_{3-y}Fe_ySn_2S_2$ grown crystals. The main phase of

the obtained crystals is the shandite of the $R\bar{3}m$ structure symmetry. Very small by-products, $CoSn_2$ and/or Sn- or Pb-fluxes, can be easily removed from the surface by polishing, as seen in the bottom inset of Fig. 1(b). The shown low reliability *R*-factors and goodness-fit-indicator *S* indicate the satisfactory Rietveld refinement.

The refined lattice parametres of In- and Fe-substituted Co-shandite are shown Fig. 1(c). In contrast to $Co_{3-y}Fe_ySn_2S_2$ of a limited y ($y \leq 0.5$), the In concentration dependences of a and c of $Co_3Sn_{2-x}In_xS_2$ ($0 < x \leq 2$) are anisotropic and do not obey the Vegard's law. The lattice parameter c and the unit cell volume increases monotonically with x, with small kink in c at $x \sim 0.8$, whereas a shows a linear decrease until $x \sim 0.8$ and almost remains constant for higher In concentration region. The unit cell volume shows identical x- and y-dependences, however, large enhancement in c/a is observed for In-substitution. Indeed, a partial ordering of the In-Sn atoms, the prefer of In- substitution to the $M1$-site, was found by a recent neutron diffraction experiment [36]. The enhancement of the trigonal distortion in the In-substituted $Co_3Sn_{2-x}In_xS_2$ was explained

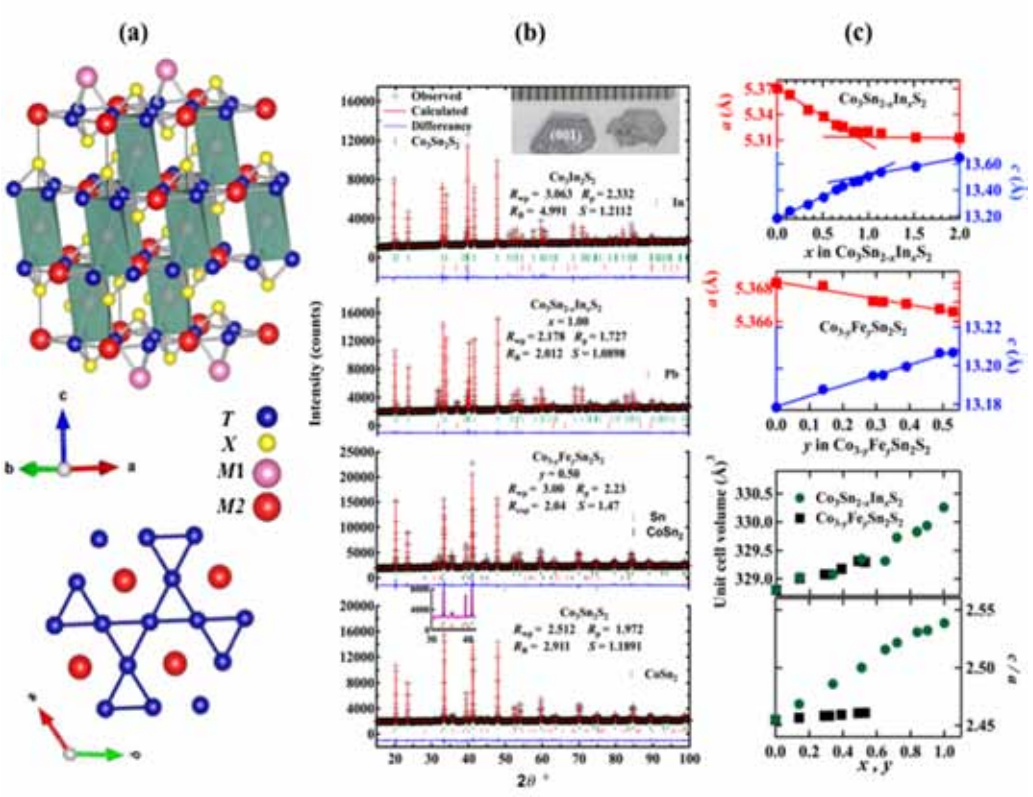

Figure 1: (a) The crystal structure of $T_3M_2X_2$ shandite showing the trigonal antiprismatic polyhedra of the inter-layers $M1$ atoms generated by 6 T atoms metallic layers of 2D kagomé sub-lattices of T and triangular sub-lattices of $M2$ atoms shown at the bottom. These structures were drawn using the VESTA software [22]. (b) Powder XRD diffraction patterns of selected $Co_3Sn_{2-x}In_xS_2$ and $Co_{3-y}Fe_ySn_2S_2$ single crystals measured at room temperature. Observed (black crosses), refined patterns using the Rietveld method (red) and differences between them (blue) are shown. Bragg reflection angles are indicated as vertical bars. The reliability *R*-factors as well as the goodness-fit-indicator *S* are indicated for each pattern. Inset in the lowest panel shows the absence of the highest peak of $CoSn_2$ in normalized patterns of well-polished single crystals of $Co_3Sn_2S_2$. The inset of the highest panel show images of grown single crystals on a mm scale of (001)-flat planes. (c) Lattice effects of In- and Fe-substitution indicated by the XRD refinement: a and c lattice parameters, unit cell volume and c to a ratio as functions of compositions [32,33]. Lines are for eye-guidance.

by the anisotropy of the In 5*p*-orbitals in DFT model calculations [1], which can also explain the smallness of the enhancement of trigonal distortion in $Co_{3-y}Fe_ySn_2S_2$.

3.2 Quasi-two-dimensional magnetism in Co-based shandites

The temperature dependences of the magnetization, M, of $Co_3Sn_{2-x}In_xS_2$ and $Co_{3-y}Fe_ySn_2S_2$ are shown at magnetic field $H = 1000$ Oe applied along and perpendicular to the c-axis, M_c and M_{ab}, for indicated x and y in Figs. 2(a - c). In consistence with literature [2,23-25], a ferromagnetic transition occurs around $T_C \sim 174$ K for $Co_3Sn_2S_2$, strong axial anisotropy has been observed below T_C. The ferromagnetic order is suppressed by In- or Fe-substitutions. Our recently reported results [32,33,35] using the grown single crystals demonstrate the observation of ferromagnetic order collapse around $x_c \sim 0.8$ in $Co_3Sn_{2-x}In_xS_2$, while the collapse of the ferromagnetic order is not found in $Co_{3-y}Fe_ySn_2S_2$ until its solubility limit $y_{max} \sim 0.5$. Nevertheless, similar (virtual) critical concentration ($y_c \sim 0.8$) is expected because of the similarity of the suppression of the ferromagnetism below y_{max} to that in $Co_3Sn_{2-x}In_xS_2$. Moreover, the magnetization data shows preservation of the strong magnetic anisotropy in the ferromagnetic regime of $Co_3Sn_{2-x}In_xS_2$ and $Co_{3-y}Fe_ySn_2S_2$. The magnetization of $Co_3Sn_{2-x}In_xS_2$ with higher x clearly shows a Pauli paramagnetic behavior, as seen in Fig. 2(c). The insets of Figs. 2(a) and (b) show the inverse susceptibility along the c-axis of $Co_3Sn_{2-x}In_xS_2$ and $Co_{3-y}Fe_ySn_2S_2$, respectively, showing the Curie-Weiss (CW) type paramagnetic behavior above T_C [35]. The data has been fitted by a modified CW Law, $\chi = \chi_0 + C/(T - \theta_W)$, where χ_0, C and θ_W represent a temperature independent Pauli paramagnetic term, the Curie constant and the Weiss temperature, respectively. The observed magnetic susceptibility behaviors above T_C well fit eq. (1) as shown in the inset figures by solid

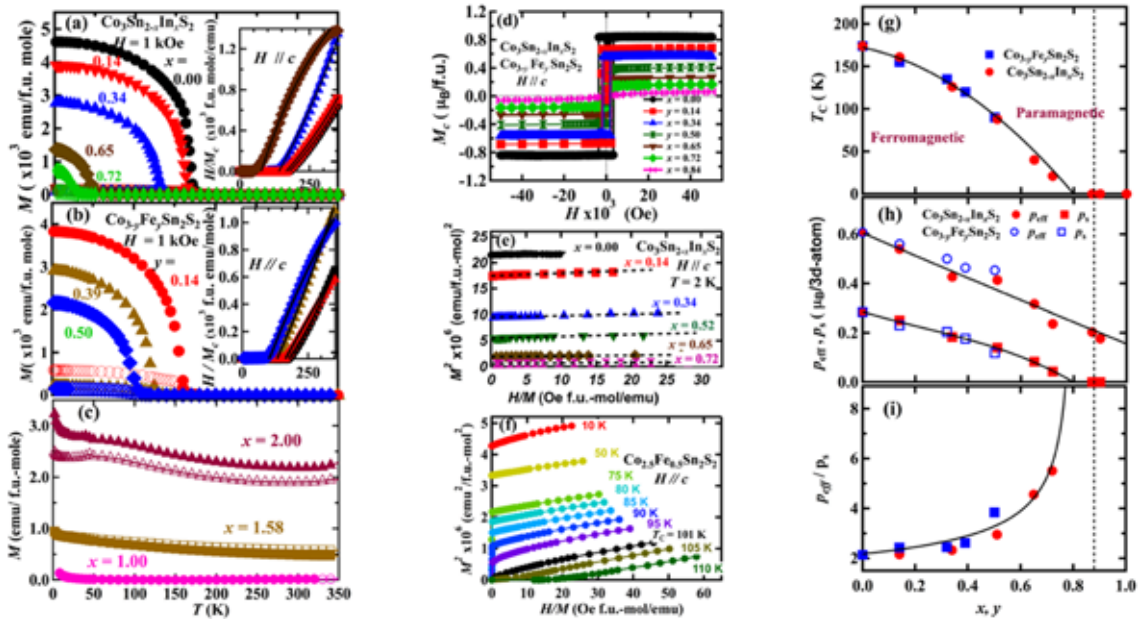

Figure 2: Static magnetic properties [35]: Temperature dependences of the static magnetization, $M(T)$, and inverse susceptibility, $H/M(T)$, for (a) and (c) $Co_3Sn_{2-x}In_xS_2$ and (b) $Co_{3-y}Fe_ySn_2S_2$ of indicated x and y, at magnetic field $H = 1$ kOe applied along (closed) and perpendicular (open) to the c-axis. (d) Magnetization hysteresis loops, Arrot plots for (d) $Co_3Sn_{1.48}In_{0.52}S_2$ at 2K and (f) $Co_{2.5}Fe_{0.5}Sn_2S_2$ at and around T_C. Fe- and In-concentration dependencies of the static magnetic parameters; (g) T_C, (h) the spontaneous moment p_s and effective moment p_{eff} per magnetic atom and (i) p_{eff}/p_s. Solid lines are for eye guidance.

lines. The effective magnetic moment in the paramagnetic state p_{eff} was estimated from $C = N_{\mathrm{A}}\mu_{\mathrm{B}}^2 p_{\mathrm{eff}}^2/3k_{\mathrm{B}}$, where N_{A}, μ_{B} and k_{B} are the Avogadro's number, Bohr magneton and Boltzmann constant, respectively[35].

The magnetic hysteresis loops of $Co_3Sn_{2-x}In_xS_2$ and $Co_{3-y}Fe_ySn_2S_2$ have been measured systematically with applying magnetic fields along and perpendicular to the easy *c*-axis at 2 K. In contrast to $M_{ab}(H)$, square-shaped hysteresis curves were observed in $M_c(H)$, presented for representative *x* and *y* in Fig. 2(d), which confirms according to the Stoner-Wohlfarth (SW) model that the easy axis is *c*-axis. The values of T_{C} and the spontaneous magnetic moment at 2 K, which can be considered to be that at T = 0 K, p_{s}, of each concentration of $Co_3Sn_{2-x}In_xS_2$ and $Co_{3-y}Fe_ySn_2S_2$ have been determined by employing the well-known Arrott plots, $M^2(T, H)$ vs. $H/M(T, H)$, at various temperatures and at 2K, respectively. Figures 2(e) and (f) show Arrott plots of the magnetically ordered samples of $Co_3Sn_{2-x}In_xS_2$ at 2 K and at various temperatures for $Co_{2.5}Fe_{0.5}Sn_2S_2$, respectively.

The In- and Fe-concentration dependences of the magnetic parameters T_{C}, p_{eff} and p_{s} are shown in Figs. 2(g - i). We have reported that the almost identical behavior against the In- and Fe-concentrations of the magnetic parameters in the In- and Fe-substituted systems indicates that the electron number, rather than crystal structure effects, is the most dominant parameter to control the magnetism in the Co-shandites [32,35]. The divergent behavior of $p_{\mathrm{eff}}/p_{\mathrm{s}}$ as approaching to x_{c} indicate the itinerant electron nature of the magnetism of the Co-based shandites [35]. The significance of electron counts to the magnetism and the contribution of the 3*d* (Co) and 5*p* (Sn) atoms to DOS at the Fermi level in shandite compounds are predicted based on reported band structure calculations [1,27,29,37].

We have also reported the highly Q2D itinerant electron magnetism in Co-shandites based on an analysis of the magnetization data using phenomenological Q2D spin fluctuation theory [38]. The zero-temperature magnetization is derived in this theory in the form of the Arrott plot with the assumption of the total spin fluctuation conservation: $M^2(T,H) = M_0^2(T) + \xi[H/M(T,H)]$, $\xi = N_0^3(2\mu_{\mathrm{B}})^4/F_1 k_{\mathrm{B}}$ and $F_1 = 4T_1^2/15T_0$, where M_0, N_0 and *g* are the magnetization at H = 0, number of the magnetic atoms and *g* factor, respectively. T_1 and T_0 are measures of the spin fluctuation spectrum in wave vector and energy spaces and F_1 is the parameter related with the slope of the Arrott plot ξ. The estimated spin fluctuation parameters, T_1 and F_1, from the experimental data of $Co_3Sn_{2-x}In_xS_2$ and $Co_{3-y}Fe_ySn_2S_2$ by employing these equations are presented in Fig. 3(a).

When $T_{\mathrm{C}} \ll T_0$ and by introducing a parameter $\varepsilon = \sqrt{m/m'}$, where *m* and *m'* are the in-plane and out-of-plane effective masses of electrons, respectively, the following relations are also derived [38-40]: $p_{\mathrm{S}}^2 = (20\,T_0/T_1)C_{4/3}(t_{\mathrm{C}})^{4/3}$ and $\left(\frac{P_{\mathrm{eff}}}{P_{\mathrm{S}}}\right)^2 = \frac{3-\varepsilon^2}{20\,t_{\mathrm{c}}\,S(0,\ t_{\mathrm{c}}/\varepsilon^3)}\left(\frac{dY}{dt}\right)^{-1}$. Here $t_{\mathrm{C}} = T_{\mathrm{C}}/T_0$ is a scaled Curie temperature, $C_{4/3}$ = 1.00608….and *t* and *Y* are the scaled temperature T/T_0 and scaled inverse susceptibility $N_{\mathrm{o}}/2k_{\mathrm{B}}T_{\mathrm{A}}\chi$, respectively. $S(Y, t_{\mathrm{C}}/\varepsilon^3)$ is related to the amplitude of the thermal spin fluctuation. The scaled temperature dependences of *Y* and *S* are evaluated from the self-consistent equations [41]. ε = 1 and 0 correspond to the ideal 3D and 2D cases of itinerant electron magnetism, respectively. Figure 3(b) shows the numerically calculated results of the t_{C}-dependence of $p_{\mathrm{eff}}/p_{\mathrm{s}}$ with several ε as well as the experimental data of typical reported itinerant electron magnets. The experimental data of the Co-based shandites roughly coincide with the result with small value of ε, ε = 0.05, which clearly indicates the highly Q2D nature of the magnetism in Co-shandites.

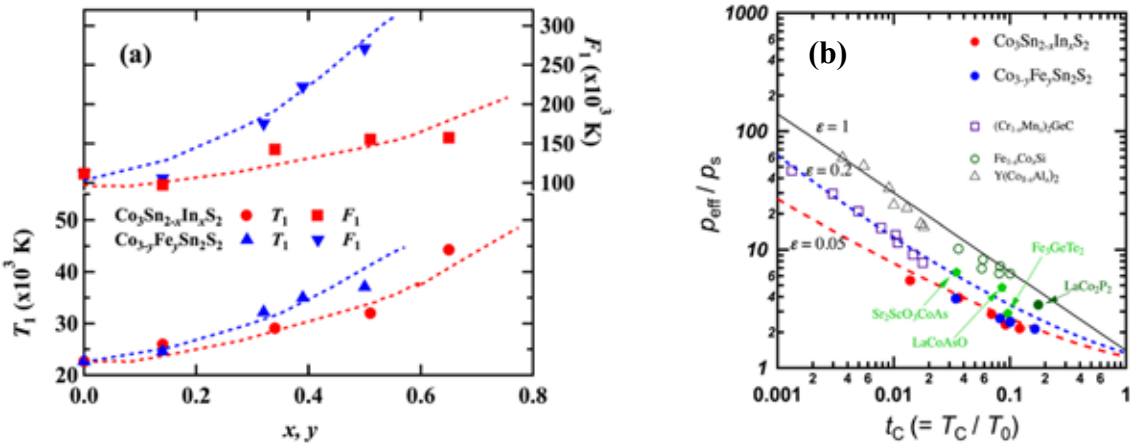

Figure 3: Spin fluctuation parameters of shandite ferromagnets [35]: (a) compositional variation of T_1 and F_1 (see text), and (b) the generalized Rhodes–Wohlfarth plot, p_{eff}/p_s versus t_C (= T_C/T_0), in a double logarithmic scale (Deguchi-Takahashi plot) of magnetic shandites compared to other itinerant electron ferromagnets [38].

3.3 Low-field equilibrium anomalous magnetic phase in the vicinity of T_C

Our recently reported precise measurements of the magnetization and the AC susceptibility for $Co_3Sn_2S_2$ has provided an approach to its low-field *H*-*T* phase diagrams. For the first time we have revealed the presence of a zero- and low-field anomalous equilibrium phase just below T_C [4]. Characteristic magnetic transitions, apart from the transition at T_C, were found at low fields where the ZFC and FC magnetizations separate from each other. Hump-like anomaly in the FC process at T_A ($T_A \approx 126$ K with applying $H = 5$ Oe) and a dip in the ZFC process in between T_A and T_C have been observed in $M_c(T, H)$ and $M_{ab}(T, H)$, shown in Figs. 4(a) and (b), respectively. The ZFC $M_{ab}(T, H)$ also shows a hump at T_A at low fields ($\leq$ 150 Oe) as seen in the inset of Fig. 4(b). The anomalies in $M_c(T, H)$ are observed at fields below the saturation fields of $Co_3Sn_2S_2$ [3], ~ 400 Oe, and still observable above 400 Oe in $M_{ab}(T, H)$. The anomalous transitions below T_C are still preserved with the chemical substitution by Fe for Co or In for Sn in $Co_{3-y}Fe_ySn_2S_2$ and $Co_3Sn_{2-x}In_xS_2$ ferromagnets, as shown for $x = 0.52$, in Fig. 4(c), and for $y = 0.5$, in Fig. 4(c) inset. The hump anomaly in the FC-$M_c(T)$ is hardly observed for $Co_{2.5}Fe_{0.5}Sn_2S_2$ single crystal.

We have reported the observations of characteristic features in the ZFC and FC real and imaginary parts of the AC susceptibility, $\chi'(T, H, f)$ and $\chi''(T, H, f)$, at under 1 Oe AC field, of a wide frequency range from 0.01 to 1000 Hz, and low DC fields applied alone *c*-axis [4]. $\chi'(T, f)$ shows a sharp peak at T_C, a hump at T_A, and a dip between T_A and T_C for all frequencies at zero and low fields, as shown for fields of 0, 150 Oe in Figs. 4(d) and (e), respectively. As well as in DC magnetization, the hump and the broad dip are absent in $\chi'(T, f)$ at the fields higher than 400 Oe, as clearly observed at 600 Oe in Fig. 4(f). The anomaly at T_C in $\chi'(T, f)$ is rather broad at 600 Oe, suggesting different natures at the low and high fields. More pronounced features are pronounced in the imaginary part of the AC susceptibility, χ''. Figures 4(g), (h) and (i) show $\chi''(T, f)$ at H = 0, 150 and 600 Oe, respectively. At low fields, χ'' that is almost absent above T_C shows a rapid increase at T_C and the T_A-anomalies in the distinct $\chi''(T, f)$ below T_C are observed only at 1 Hz. At 600 Oe, χ'' is almost absent regardless of temperature and frequency. These features indicate that the spin dynamics slow down to the experimental time window of 0.001–1 s only between T_A and T_C and at low fields.

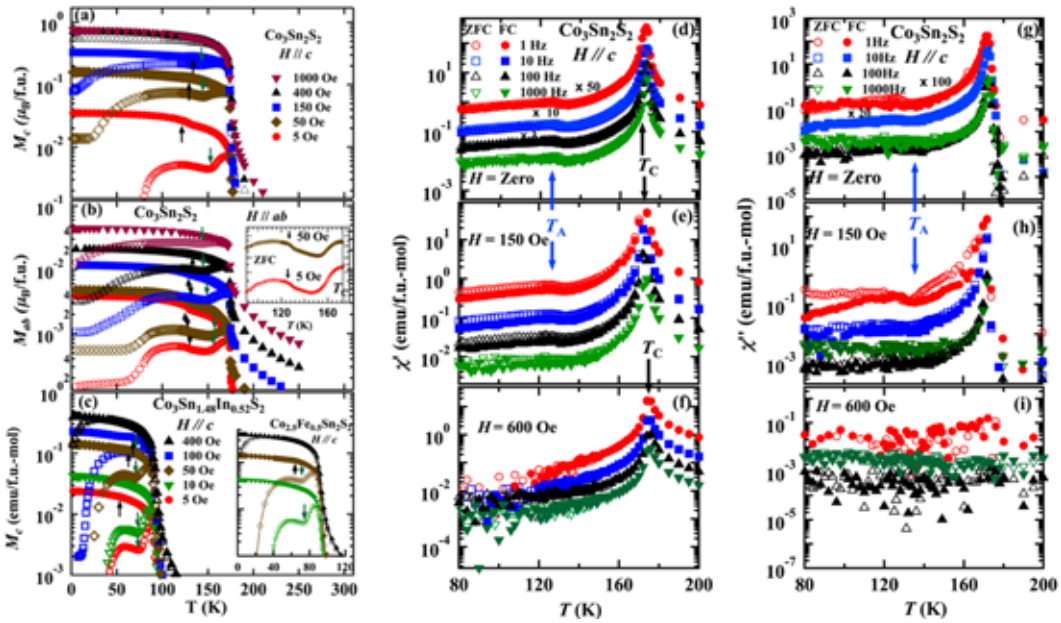

Figure 4: Typical temperature dependences of ZFC (open) and FC (closed) magnetizations, $M(T, H)$, χ' and χ'', measured at different magnetic fields [4]: $M(T, H)$ (a) along and (b) perpendicular to the *c*-axis for $Co_3Sn_2S_2$ and (c) along the *c*-axis for $Co_3Sn_{1.48}In_{0.52}S_2$. Inset of (b) shows a magnification of the ZFC $M_{ab}(T)$ measured at very low fields. Inset of (c) shows data of $Co_{2.5}Fe_{0.5}Sn_2S_2$. Vertical arrows indicate the transition temperature, T_A, and the broad dip (see text). (d - f) χ' and (g - i) χ'' of $Co_3Sn_2S_2$ measured at represenative frequencies for fields applied along the *c*-axis.

Based on the magnetization and AC susceptibility data described above, we have established the *H*–*T* phase diagrams of $Co_3Sn_2S_2$ [4], shown here for H // c and H // ab in Figs. 5(a) and (b), respectively. The *H*-*T* region surrounded by T_A and T_C is denoted as the A phase, which is not closed in Fig. 5(b) because the in-plane magnetization hardly saturates in $Co_3Sn_2S_2$. Following the established phase diagram, the frequency dependences of the AC susceptibility were carefully measured at different temperatures to study the spin relaxation and see the slow spin dynamics in the A phase. We found that χ' are weakly frequency-dependent, and correspondingly, χ'' are almost absent, below T_A while both become pronouncedly frequency-dependent with approaching the high-temperature boundary between the A and paramagnetic phases. The magnitudes of both χ' and χ'' are suppressed and becomes almost frequency-independent above the high-field and/ or temperature boundary of the A phase.

To evaluate the spin dynamics in the A phase, we have employed the phenomenological Cole-Cole formalism [42,43]: $\chi(\omega) = \chi(\infty) + A_0/[1 + (i\omega\tau_0)^{1-\alpha}]$, with $\chi(\omega) = \chi'(\omega) + i\,\chi''(\omega)$ and $A_0 = \chi(0) - \chi(\infty)$, where $\chi(0)$ and $\chi(\infty)$ are the isothermal and adiabatic susceptibilities, $\omega = 2\pi f$ is the angular frequency, τ_0 is the relaxation time, and α is a measure of the distribution of the relaxation time. The experimental data (symbols) and fitting results using Cole-Cole formalism (solid lines) at different frequencies are displayed in the form of χ'' vs. f and χ'' vs. χ' (the Cole-Cole plot) for H = 150 Oe at several temperatures and for several fields at 172 K in Figs. 5(c) and (d) and Figs. 5(e) and (f), respectively. Although, the Cole-Cole formalism is not valid at low frequencies, the fitting results in an estimated α, little varying at around 0.6 indicating a significant distribution of relaxation times and the characteristic frequency, $f_0 = 1/\tau_0$, drastically decreases with decreasing temperature at around T_C, but almost field-independent, as seen in the insets of Figs. 5(e)

and (f), respectively. An estimated f_0 lower than 0.1 Hz below ~171 K markedly indicate slow spin dynamics only in the anomalous phase with characteristic relaxation times longer than 10 s. The slow relaxation inside the A phase indicates a kind of spin-frozen state in the A phase.

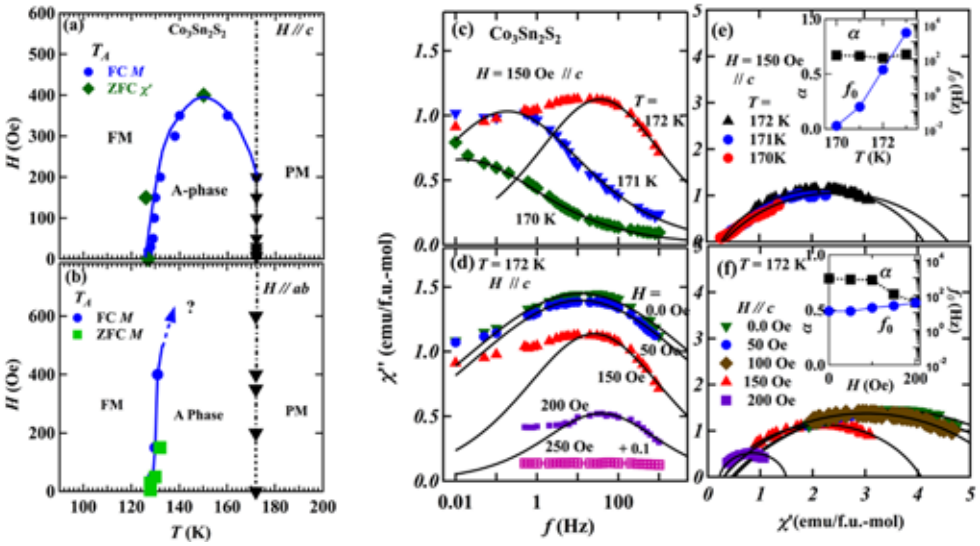

Figure 5: Anomalous phase of slow spin dynamics below T_C of $Co_3Sn_2S_2$[4]**:** Magnetic *H-T* phase diagrams of $Co_3Sn_2S_2$ for fields applied (a) along and (b) perpendicular to the *c*-axis. Solid curves are for the eye guidance. (c) and (d) the frequency dependences of ZFC- χ", and (c) and (d) the cole-cole plot, χ' versus χ", of $Co_3Sn_2S_2$ at 170–172 K (close to T_C) for 150 Oe and at $T_C \approx 172$ K for different fields applied along the *c*-axis, respectively. Solid lines in (c)–(f) represent fittings resuls (see text). Insets of (e) and (f) show the fitting parameters, α and f_0, as functions of temperature at $H = 150$ Oe and as functions of applied field at $T = 172$ K, respectively.

We have excluded the spin glass-like state, given the absence of disorder and the fast relaxation below T_A, and a non-equilibrium phenomenon such as domain-wall motions, as described in our recent publication [4], to be the origin of the observed anomalous magnetic transitions. We attributed the anomalous A phase in Co-shandites to possibly noncolinear spin structures, such as the topologically protected skyrmions, stabilized by the DM interaction and/or spin frustration, if antiferromagnetic component of the exchange interaction coexists. Both are inherent to the kagomé lattice as described in Sec. 1. In chiral skyrmion hosts [44-47], the distribution of relaxation times and slow spin dynamics in the experimental time scale of χ_{ac} near T_C have actually been observed. One of the observable multi-**q** states in centrosymmetric lattices; stripe domains, soft and hard magnetic bubbles, biskyrmions, etc., can be realized [48] and may explain the nature of the A phase in $Co_3Sn_2S_2$ that extends to Zero fields. We suggest further experiments such as the small-angle neutron scattering (SANS), spin-polarized scan tunneling microscopy (STM) or Lorentz TEM microscopy to shed light on the nature of $Co_3Sn_2S_2$ magnetism.

4. Conclusion

Single crystals of two series-compounds of Co-based shandites, $Co_3Sn_{2-x}In_xS_2$ ($0 < x \leq 2$) and $Co_{3-y}Fe_ySn_2S_2$ ($y \leq 0.5$), were successfully grown using a flux method. The structure was investigated by powder x-ray diffraction and the crystal structure parameters were refined by the Rietveld analysis. Furtherly,

the crystals were characterized using wavelength-dispersive x-ray spectroscopy and Laue x-ray spectroscopy. Comprehensive magnetization measurements were performed using the grown single crystals of Co-based shandites. A strongly-uniaxial anisotropic ferromagnetic order of $Co_3Sn_2S_2$ below T_C ~173 K is suppressed identically by In- and Fe-substitutions indicating significance of the electron count. The ferromagnetic-nonmagnetic quantum phase transition was found at around x_c (y_c) ~ 0.8. Analyses of the magnetizations based on the extended Q2D spin fluctuation theory clearly revealed a highly Q2D itinerant electron magnetism of Co-shandites. Low-field-dependent anomalous transitions in the magnetization and AC susceptibility indicating an equilibrium unconventionally-ordered phase (A phase) have been observed below T_C. The frequency-distributed spin relaxation process with characteristic relaxation times of the order of several seconds has been observed in the A phase. Our results arise a lot of questions that can be answered by further theoretical and experimental investigations of the nature of Co-shandite magnetic states.

References

[1] F. Pielnhofer, J. Rothballer, P. Peter, W. Yan, F. M. Schappacher, R. Pöttgen, and R. Weihrich, Z. Anorg. Allg. Chem. **640**, 286 (2014).

[2] W. Schnelle, A. Leithe-Jasper, H. Rosner, F.M. Schappacher, R. Pöttgen, F. Pielnhofer, and R. Weihrich, Phys. Rev. B **88**, 144404 (2013).

[3] M. A. Kassem, Y. Tabata, T. Waki, and H. Nakamura, J. Phys. Soc. Jpn. **85**, 64706 (2016).

[4] M. A. Kassem, Y. Tabata, T. Waki, and H. Nakamura, Phys. Rev. B 1 (2017).

[5] H. Ohta, C. Michioka, and K. Yoshimura, J. Phys. Soc. Japan **79**, 54703 (2010).

[6] H. Sugawara, K. Ishida, Y. Nakai, H. Yanagi, T. Kamiya, Y. Kamihara, M. Hirano, and H. Hosono, J. Phys. Soc. Japan **78**, 113705 (2009).

[7] Z. Liu, T. Waki, Y. Tabata, and H. Nakamura, Phys. Rev. B **89**, 54435 (2014).

[8] H. Ohta, D. Noguchi, K. Nabetani, and H. Aruga Katori, Phys. Rev. B **88**, 94441 (2013).

[9] H. Ohta and K. Yoshimura, Phys. Rev. B **79**, 184407 (2009).

[10] F. L. Ning, K. Ahilan, T. Imai, A. S. Sefat, M. A. McGuire, B. C. Sales, D. Mandrus, P. Cheng, B. Shen, and H. -H. Wen, Phys. Rev. Lett. **104**, 37001 (2010).

[11] S. Sachdev, Science **288**, 475 (2000).

[12] L. Balents, Nature **464**, 199 (2010).

[13] H. T. Diep, *Magnetic Systems with Competing Interactions: Frustated Spin System* (World Scientific, Singapore, 1994).

[14] Y. Taguchi, Y. Oohara, H. Yoshizawa, N. Nagaosa, and Y. Tokura, Science **291**, 2573 (2001).

[15] Y. Machida, S. Nakatsuji, S. Onoda, T. Tayama, and T. Sakakibara, Nature **463**, 210 (2010).

[16] D. Grohol, K. Matan, J.-H. Cho, S.-H. Lee, J.W. Lynn, D.G. Nocera, and Y.S. Lee, Nat. Mater. **4**, 323 (2005).

[17] M. Elhajal, B. Canals, and C. Lacroix, Phys. Rev. B **66**, 14422 (2002).

[18] I. Dzyaloshinsky, J. Phys. Chem. Solids **4**, 241 (1958).

[19] T. Moriya, Phys. Rev. **120**, 91 (1960).

[20] K. Matan, B. M. Bartlett, J. S. Helton, V. Sikolenko, S. Mat'aš, K. Prokeš, Y. Chen, J. W. Lynn, D. Grohol, T. J. Sato, M. Tokunaga, D. G. Nocera, and Y. S. Lee, Phys. Rev. B **83**, 214406 (2011).

[21] U. K. Rößler, A.N. Bogdanov, and C. Pfleiderer, Nature **442**, 797 (2006).

[22] K. Momma and F. Izumi, J. Appl. Crystallogr. **41**, 653 (2008).

[23] R. Weihrich, I. Anusca, and M. Zabel, Z. Anorg. Allg. Chem. **630**, 1767 (2004).

[24] A. Umetani, E. Nagoshi, T. Kubodera, and M. Matoba, Phys. B Condens. Matter **403**, 1356 (2008).

[25] X. Lin, S.L. Bud'ko, and P.C. Canfield, Philos. Mag. **92**, 2436 (2012).
[26] R. Weihrich and I. Anusca, Z. Anorg. Allg. Chem. **632**, 1531 (2006).
[27] J. Rothballer, F. Bachhuber, F. Pielnhofer, F.M. Schappacher, R. Pöttgen, and R. Weihrich, Eur. J. Inorg. Chem. **2013**, 248 (2013).
[28] Y. Sakai, R. Tanakadate, M. Matoba, I. Yamada, and N. Nishiyama, J. Phys. Soc. Jpn. **84**, 44705 (2015).
[29] J. Corps, P. Vaqueiro, A. Aziz, R. Grau-Crespo, W. Kockelmann, J. -C. Jumas, and A. V. Powell, Chem. Mater. **27**, 3946 (2015).
[30] M. Fujioka, T. Shibuya, J. Nakai, K. Yoshiyasu, Y. Sakai, Y. Takano, Y. Kamihara, and M. Matoba, Solid State Commun. **199**, 56 (2014).
[31] P. Mangelis, P. Vaqueiro, J. -C. Jumas, I. da Silva, R. I. Smith, and A. V. Powell, J. Solid State Chem. **251**, 204 (2017).
[32] M. A. Kassem, Y. Tabata, T. Waki, and H. Nakamura, J. Solid State Chem. **233**, 8 (2016).
[33] M. A. Kassem, Y. Tabata, T. Waki, and H. Nakamura, J. Cryst. Growth **426**, 208 (2015).
[34] K. Izumi, F. Momma, Solid State Phenom. **130**, 15 (2007).
[35] M. A. Kassem, Y. Tabata, T. Waki, and H. Nakamura, J. Phys. Soc. Japan **85**, 64706 (2016).
[36] J. Rothballer, F. Bachhuber, S. M. Rommel, T. Söhnel, and R. Weihrich, RSC Adv. **4**, 42183 (2014).
[37] F. Pielnhofer, A. S. Tragl, J. Rothballer, and R. Weihrich, Z. Naturforsch. **69B**, 55 (2014).
[38] Y. Takahashi, *Spin Fluctuation Theory of Itinerant Electron Magnetism* (Springer, Berlin, 2013).
[39] Y. Takahashi, J. Phys. Soc. Japan **55**, 3553 (1986).
[40] Y. Takahashi, J. Phys. Condens. Matter **9**, 10359 (1997).
[41] To distinguish from the symbols used here for Fe concentration and temperature as *y* and *T*, respectively, we introduce the scaled ynverse suseptibility parameter and the parameter related with the amplitude of thew thermal spin fluctuation as *Y* and *S*, respectively, instead of *y* and *T* used for the same parameters in the spin fluctuation theory presented in Ref. 40.
[42] K. S. Cole and R. H. Cole, J. Chem. Phys. **9**, 341 (1941).
[43] C. Dekker, A. F. M. Arts, H. W. de Wijn, A. J. van Duyneveldt, and J. A. Mydosh, Phys. Rev. B **40**, 11243 (1989).
[44] A. Bauer and C. Pfleiderer, Phys. Rev. B **85**, 214418 (2012).
[45] F. Qian, H. Wilhelm, A. Aqeel, T. T. M. Palstra, A. J. E. Lefering, E. H. Brück, and C. Pappas, Phys. Rev. B **94**, 64418 (2016).
[46] L. J. Bannenberg, A. J. E. Lefering, K. Kakerai, Y. Onose, Y. Endoh, Y. Tokura, and C. Pappas, Phys. Rev. B **94**, 134433 (2016).
[47] I. Levatić, V. Šurija, H. Berger, and I. Živković, Phys. Rev. B **90**, 224412 (2014).
[48] X. Yu, Y. Tokunaga, Y. Taguchi, and Y. Tokura, Adv. Mater. **29**, 1603958 (2017).

Curriculum Vitae

Mohamed Abdelkareem Ali Ahmed Kassem

Lecturer, Department of Physics, Assiut University, Egypt

2004 Bachelor of Science, Department of Physics, Assiut University, Egypt

2011 Master of Science, Department of Physics, Assiut University, Egypt

2017 Doctor of Engineering, Department of Materials Science and Engineering, Kyoto University

2017 – present Lecturer, Department of Physics, Assiut University, Egypt